DISCLAIMER

This report was prepared as an account of work sponsored by an agency of the United States Government. Neither the United States Government nor any agency thereof, nor any of their employees, makes any warranty, express or implied, or assumes any legal liability or responsibility for the accuracy, completeness, or usefulness of any information, apparatus, product, or process disclosed, or represents that its use would not infringe privately owned rights. Reference herein to any specific commercial product, process, or service by trade name, trademark, manufacturer, or otherwise does not necessarily constitute or imply its endorsement, recommendation, or favoring by the United States Government or any agency thereof. The views and opinions of authors expressed herein do not necessarily state or reflect those of the United States Government or any agency thereof. Reference herein to any social initiative (including but not limited to Diversity, Equity, and Inclusion (DEI); Community Benefits Plans (CBP); Justice 40; etc.) is made by the Author independent of any current requirement by the United States Government and does not constitute or imply endorsement, recommendation, or support by the United States Government or any agency thereof.

LA-UR-25-30084

Approved for public release; distribution is unlimited.

Title: One-Dimensional Multi-Velocity Capabilities for Arbitrary Lagrangian-Eulerian Normal Contact Mechanics

Author(s): Delgado, Conrad Joseph
Manolas, Spiros Kiriakos
Vaughn-Kukura, Nathanial Joseph
Shashkov, Mikhail Jurievich

Intended for: Report

Issued: 2025-10-10

One-Dimensional Multi-Velocity Capabilities for Arbitrary Lagrangian-Eulerian Normal Contact Mechanics

Conrad Delgado[1,2], Spiros Manolas[1,3], Nathanial Vaughn-Kukura[1], Mikhail Shashkov[1]

[1] X-Computational Physics, Los Alamos National Laboratory, Los Alamos, New Mexico, 87544, USA
[2] University of Illinois Urbana-Champaign, Urbana, Illinois, 61820, USA
[3] Stony Brook University, Stony Brook, New York, 11794, USA

Abstract

Lagrangian and Arbitrary Lagrangian Eulerian (ALE) hydrodynamics codes such as FLAG form the backbone of many mission-critical multi-physics simulations at Los Alamos National Laboratory. Critical to preforming high fidelity simulations with these codes are Lagrangian and ALE contact algorithms, which allow materials to collide, slide, and separate throughout a simulation. Current Lagrangian and ALE contact algorithms do not have the ability to track individual material velocities across sub-zonal material interfaces, which is essential to integrating contact and sliding with a diverse range of multi-physics capabilities. We develop such an ALE contact algorithm which has the capability to operate on sub-zonal material interfaces and on one simply connected mesh in a single dimension. This is performed by evolving each material within a lagrangian mesh individually, and then correcting the position of each material with a contact force, calculated using the overfill between materials, so that material polygon and nodal positions align with that of a single-velocity mesh. An optional first-order remapping procedure to a universal mesh may then be used so that void may be removed or injected from a cell. Our algorithm is tested on a variety of one-dimensional test cases, and is able to converge to analytical solutions when available, as well as conserve total energy. Future work involves extending our results to two and three dimensions, implementing a higher order remapping procedure, and implementing the algorithm in FLAG.

1 Introduction

Hydrodynamics simulations often involve a variety of phenomena, such as large deformations, contact mechanics, and multi-physics capabilities. Current methods, however, can model at most two of these three capabilities, which presents a pressing issue, as many multi-physics simulations rely on high-fidelity contact mechanics and large deformation mechanics. Multi-mesh contact methods

such as slidelines and overset meshes, while able to model large deformations and contact mechanics, are lacking in multi-physics capabilities because of their usage of more than one mesh [7]. Current Arbitrary Lagrange-Eulerian (ALE) methods, while able to model large deformations with multi-physics capabilities, are limited in their ability to accurately model contact and sliding between materials, as their usage of a single velocity that is shared between materials causes them to stick together [3]. We propose a method to add multi-velocity capabilities to ALE hydrodynamics by allowing materials to evolve independently of one another, which is followed by a correction through a contact force.

We consider a single-dimension multi-velocity Staggered Grid Hydrodynamics (SGH) formulation wherein cell and nodal-based material quantities are first evolved in a Lagrangian timestep, that uses a predictor-corrector scheme. At the end of each predictor/corrector sub-step, contact forces, calculated from the overfill between adjacent materials, correct material polygon and nodal positions and velocities to exactly match that of a single-velocity mesh. Each Largangian timestep is followed by a first order remapping to a universal mesh with equidistant mesh nodes. The remapping procedure is used to allow void to be injected and removed from cells and to prevent cell volumes from approaching zero. The use of a purely-Lagrangian approach can lead to issues when dealing with cells filled entirely with void.

We test this approach on a variety of one dimensional test cases, showing that our results converge to analytical results (when available), and that total energy is conserved.

Our approach is limited by the remap procedure, which poses an over-constrained problem when one attempts to conserve mass, momentum, kinetic energy, internal energy, and total energy. One can, however, choose to conserve mass, momentum, and total energy through a kinetic energy fix, which perturbs potential energy in response to changes in the kinetic energy after the remap in order to conserve total energy.

This paper is structured as follows. Section 2 introduces the partial differential equations which govern the evolution of momentum and internal energy in a Lagrangian reference frame, as well as our equation of state. Section 3 introduces the Staggered Grid Hydrodynamics (SGH) formulation of our hydrodynamics simulations as well as the predictor-corrector scheme used to discretize the equations from §2. Section 4 details our approach for adding multi-velocity capabilities, detailing the step-by-step algorithm; how overfill and contact forces are calculated; and the mechanism behind our remap procedure. Section 5 shows results from running our method on a variety of test cases. Section 6 summarizes and concludes our findings.

2 Governing Equations

The partial differential equations governing momentum and internal energy are written in the Lagrangian reference frame as

$$\rho \frac{\partial u}{\partial t} + \nabla p = 0 \tag{1}$$

$$\rho \frac{\partial \varepsilon}{\partial t} + p \nabla \cdot u = 0 \tag{2}$$

where ρ is the density, p is the pressure, ε is the specific internal energy, and u is the velocity [2]. In the Lagrangian reference frame the mass of a fluid parcel is constant, so the specific volume τ can be calculated as $\tau = V/M = 1/\rho$.

The pressure is a function of the density and specific internal energy $p = \mathcal{P}(\rho, \varepsilon) = \mathcal{P}(\tau, \varepsilon)$, which is given by the stiffened gas equation of state as

$$p = \rho\varepsilon(\gamma - 1) - \gamma p_\infty. \tag{3}$$

The stiffened gas sound speed cs is given as

$$cs = \sqrt{\frac{\gamma(p + p_\infty)}{\rho}}. \tag{4}$$

The stiffened gas equation of state was chosen for its ability to faithfully model both gases and liquids. For ideal gases, $p_\infty = 0$.

3 Staggered Grid Hydrodynamics (SGH)

For our staggered discretization of the governing equations we use the predictor-corrector scheme detailed in [2]. Thermodynamic variables exist at cell-centers and kinematic variables exist at cell edges. Cell-centered quantities are denoted with half indices $(\cdot)_{i+1/2}, (\cdot)_{i-1/2}, (\cdot)_{i+3/2}$, while node-centered quantities are denoted with whole indices $(\cdot)_i, (\cdot)_{i-1}, (\cdot)_{i+1}$. The cell-centered quantities include the cell mass $M_{i+1/2}$, cell volume $V_{i+1/2}$, cell density $\rho_{i+1/2}$, cell specific volume $\tau_{i+1/2}$, cell specific internal energy $\varepsilon_{i+1/2}$, cell pressure $p_{i+1/2}$, and cell sound speed $cs_{i+1/2}$. The node-centered quantities include the mesh node location x_i and $x_i + 1$, the node velocities u_i and u_{i+1}, and the node masses m_i and m_{i+1}. The cell volume $V_{i+1/2}$ can be obtained from the mesh node locations x_i and $x_i + 1$ as $V_{i+1/2} = x_{i+1} - x_i$. The cell node locations are governed by the equation

$$\frac{\mathrm{d}x_i}{dt} = u_i. \tag{5}$$

3.1 Predictor-Corrector Method

The governing equations 1, 2, and 5 can be solved using a predictor-corrector method, as described in [2]. Time levels are denoted with superscripts $(\cdot)^n$. The scheme is as follows:

Predictor

$$u_i^{n+1,*} = u_i^n - \frac{\Delta t}{m_i}(p_{i+1/2}^n - p_{i-1/2}^n) \tag{6}$$

$$u_i^{n+1/2,*} = \frac{1}{2}(u_i^n + u_i^{n+1,*}) \tag{7}$$

$$x_i^{n+1,*} = x_i^n + \Delta t u_i^{n+1/2,*} \tag{8}$$

$$V_{i+1/2}^{n+1,*} = x_{i+1}^{n+1,*} - x_i^{n+1,*} \tag{9}$$

$$\tau_{i+1/2}^{n+1,*} = V_{i+1/2}^{n+1,*}/M_{i+1/2} \tag{10}$$

$$\varepsilon_{i+1/2}^{n+1,*} = \varepsilon_{i+1/2}^n - \frac{\Delta t}{M_{i+1/2}} p_{i+1/2}^n (u_{i+1}^{n+1/2,*} - u_i^{n+1/2,*}) \tag{11}$$

$$p_{i+1/2}^{n+1,*} = \mathcal{P}(\tau_{i+1/2}^{n+1,*}, \varepsilon_{i+1/2}^{n+1,*}) \tag{12}$$

Corrector

$$u_i^{n+1} = u_i^n - \frac{1}{2}\frac{\Delta t}{m_i}(p_{i+1/2}^n + p_{i+1/2}^{n+1,*} - p_{i-1/2}^n - p_{i-1/2}^{n+1,*}) \tag{13}$$

$$u_i^{n+1/2} = \frac{1}{2}(u_i^n + u_i^{n+1}) \tag{14}$$

$$x_i^{n+1} = x_i^n + \Delta t u_i^{n+1/2} \tag{15}$$

$$V_{i+1/2}^{n+1} = x_{i+1}^{n+1} - x_i^{n+1} \tag{16}$$

$$\tau_{i+1/2}^{n+1} = V_{i+1/2}^{n+1}/M_{i+1/2} \tag{17}$$

$$\varepsilon_{i+1/2}^{n+1} = \varepsilon_{i+1/2}^n - \frac{1}{2}\frac{\Delta t}{M_{i+1/2}}(p_{i+1/2}^n + p_{i+1/2}^{n+1,*})(u_{i+1}^{n+1/2} - u_i^{n+1/2}) \tag{18}$$

$$p_{i+1/2}^{n+1} = \mathcal{P}(\tau_{i+1/2}^{n+1}, \varepsilon_{i+1/2}^{n+1}) \tag{19}$$

In order to decrease oscillations for problems with discontinuous solutions, it is necessary to augment the pressure by an artificial viscosity. This adds extra numerical dissipation to the solution. We use the linear-plus-quadratic model of von Neumann and Richtmyer [8]

$$\Delta u_{i+1/2}^n = u_{i+1}^n - u_i^n \tag{20}$$

$$q_{i+1/2}^n = \begin{cases} 0 & \text{if } \Delta u_{i+1/2}^n \geq 0 \\ -\nu_1 \rho_{i+1/2}^n c s_{i+1/2}^n \Delta u_{i+1/2}^n + \nu_2 \rho_{i+1/2}^n (\Delta u_{i+1/2}^n)^2 & \text{otherwise} \end{cases} \tag{21}$$

where ν_1 and ν_2 are the coefficients of the linear and quadratic contributions and are given values of 1 and 0.1, respectively. The artificial viscosity is added in the predictor and corrector steps such that in the predictor $p = p + q$ and in the corrector $p = p + q$, $p^* = p^* + q$.

4 Multi-Material and Multi-Velocity

For multi-material and multi-velocity problems, thermodynamic and kinematic variables now have an additional material index, $(\cdot)_{mat}$. It is also necessary to

introduce cell-based quantities, which are not located at the cell centers or cell nodes but instead have a value for a given cell. For a cell $\mathcal{C}_i$, these include the material volume fraction $\phi_{i,mat}$, the overfill θ_i, and the material polygon volume $\mathcal{V}_{i,mat}$.

4.1 Algorithm Overview

Algorithm 1 Multi-Velocity Time-Step Evolution Algorithm

1. Evolve per material meshes using per material velocities
2. Evolve single velocity mesh using single velocity (standard SGH)
3. Compute intersection of material polygons from their per material meshes into the single velocity mesh
4. Compute the cell-based overfill on the single velocity mesh
5. Compute the node-centered contact forces from the overfill
6. Re-evolve the per material meshes using their per material velocities, now including the contact forces
7. Evolve the thermodynamic variables from the new per material meshes
8. Optionally, remap quantities to a universal mesh of interest

4.2 Overfill

After intersecting the per material mesh material polygons into the single velocity mesh, we can calculate the overfill as

$$\theta_i = \sum_{mat \in \mathcal{C}_i} \mathcal{V}_{i,mat} - V_{i+1/2} \tag{22}$$

where $\mathcal{V}_{i,mat}$ is the volume of a material mat within cell $\mathcal{C}_i$ and $V_{i+1/2}$ is the volume of cell $\mathcal{C}_i$.

4.3 Contact Forces

4.3.1 Generalized Contact Forces for Overfills in Multi-Material Cells

For the case in which overfill occurs between two materials that both occupy the same multi-material cell, a general equation for contact forces must be formulated. It is important to note that this case includes a sub-case wherein the material interface is near a node position and overfill occurs within both the cell that contains the interface and an adjacent cell; this case is treated by summing the overfills within both cells into one overfill, denoted θ_i. Consider a material mat_L which inhabits cells C_{i-1} and C_i and a material mat_R which inhabits cells

C_i and C_{i+1}, and that both materials evolve independently such that overfill occurs:

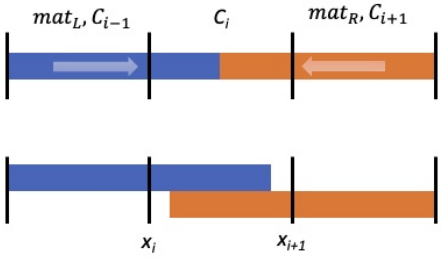

Figure 1: Overfill occurring within a multi-material cell

Before the evolution, the per material and single-velocity mesh SVM nodes at x_i and x_{i+1} are all in agreement with each other, and we denote these values x_i^n and x_{i+1}^n. After the evolution, the per material and SVM mesh nodes evolve to:

$$x_{i,mat_L}^{n+1} = \frac{\Delta t^2}{2}\frac{F_{i,mat_L}}{m_{i,mat_L}} + \Delta t \cdot u_{i,mat_L}^n \tag{23}$$

$$x_{i+1,mat_L}^{n+1} = \frac{\Delta t^2}{2}\frac{F_{i+1,mat_L}}{m_{i+1,mat_L}} + \Delta t \cdot u_{i+1,mat_L}^n \tag{24}$$

$$x_{i,mat_R}^{n+1} = \frac{\Delta t^2}{2}\frac{F_{i,mat_R}}{m_{i,mat_R}} + \Delta t \cdot u_{i,mat_R}^n \tag{25}$$

$$x_{i+1,mat_R}^{n+1} = \frac{\Delta t^2}{2}\frac{F_{i+1,mat_R}}{m_{i+1,mat_R}} + \Delta t \cdot u_{i+1,mat_R}^n \tag{26}$$

$$x_{i,SVM}^{n+1} = \frac{\Delta t^2}{2}\frac{F_{i,SVM}}{m_{i,mat_L} + m_{i,mat_R}} + \Delta t \cdot u_{i,SVM}^n \tag{27}$$

$$x_{i+1,SVM}^{n+1} = \frac{\Delta t^2}{2}\frac{F_{i+1,SVM}}{m_{i+1,mat_L} + m_{i+1,mat_R}} + \Delta t \cdot u_{i+1,SVM}^n \tag{28}$$

where

$$F_{i,mat_L} = p_{i-1/2,mat_L} - \phi_{i+1/2,mat_L} p_{i+1/2,mat_L} \tag{29}$$

$$F_{i+1,mat_L} = \phi_{i+1/2,mat_L} p_{i+1/2,mat_L} \tag{30}$$

$$F_{i,mat_R} = -\phi_{i+1/2,mat_R} p_{i+1/2,mat_R} \tag{31}$$

$$F_{i+1,mat_R} = \phi_{i+1/2,mat_R} p_{i+1/2,mat_R} - p_{i+3/2,mat_R} \tag{32}$$

$$F_{i,SVM} = p_{i-1/2,mat_L} - \phi_{i+1/2,mat_L} p_{i+1/2,mat_L} - \phi_{i+1/2,mat_R} p_{i+1/2,mat_R} \quad (33)$$

$$F_{i+1,SVM} = \phi_{i+1/2,mat_L} p_{i+1/2,mat_L} + \phi_{i+1/2,mat_R} p_{i+1/2,mat_R} - p_{i+3/2,mat_R} \quad (34)$$

Consider a material mat on nodes i and $i+1$ evolved by forces $F_{i,mat}$ and $F_{i+1,mat}$, respectively. We would like to apply the contact forces $F^C_{i,mat}$ and $F^C_{i+1,mat}$ to it, respectively, such that $x^{n+1,C}_{i,mat} = x^{n+1}_{i,SVM}$ and $x^{n+1,C}_{i+1,mat} = x^{n+1}_{i+1,SVM}$, which would require:

$$x^{n+1,C}_{i,mat} = \frac{\Delta t^2}{2} \frac{F_{i,mat} + F^C_{i,mat}}{m_{i,mat}} + \Delta t \cdot u^n_{i,mat} = x^{n+1}_{i,SVM} \quad (35)$$

$$x^{n+1,C}_{i+1,mat} = \frac{\Delta t^2}{2} \frac{F_{i+1,mat} + F^C_{i+1,mat}}{m_{i+1,mat}} + \Delta t \cdot u^n_{i+1,mat} = x^{n+1}_{i+1,SVM} \quad (36)$$

Using 35 and 36 to solve for general forms of the contact forces yields:

$$F^C_{i,mat} = \frac{m_{i,mat} F_{i,SVM}}{\sum_{mat} m_{i,mat}} + \frac{2}{\Delta t} m_{i,mat} (u^n_{i,SVM} - u^n_{i,mat}) - F_{i,mat} \quad (37)$$

$$F^C_{i+1,mat} = \frac{m_{i+1,mat} F_{i+1,SVM}}{\sum_{mat} m_{i,mat}} + \frac{2}{\Delta t} m_{i+1,mat} (u^n_{i+1,SVM} - u^n_{i+1,mat}) - F_{i+1,mat} \quad (38)$$

Using equations 37 and 38, specific per-material contact forces may be computed. It is important to note that for this case, the computation for the contact force is no longer dependent on overfill. Additionally, because of the remapping procedure described in §4.4, it may not be assumed that in the previous timestep that $u^n_{i,mat_L} = u^n_{i,mat_R} = u^n_{i,SVM}$ nor that $u^n_{i+1,mat_L} = u^n_{i+1,mat_R} = u^n_{i+1,SVM}$.

4.3.2 Contact Forces for Overfills Between Pure-Material Cells

A special case for calculating contact forces arises if only one material exists within a given cell at the beginning of a timestep. When this is the case, such a cell is called a "pure cell". When two pure cells overfill into each other, we have pure cell overfill, as seen in figure 2. It is important to note that this case includes situations where one or both of these cells additionally include a small amount of void. Consider a material mat_L which inhabits cell $\mathcal{C}_{i-1}$ and a material mat_R which inhabits the adjacent cell $\mathcal{C}_i$, and that both materials evolve independently such that overfill occurs:

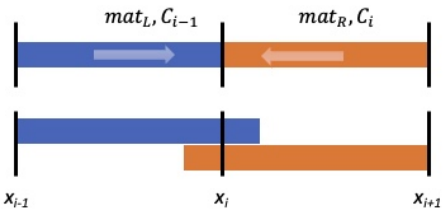

Figure 2: Overfill occurring between two adjacent pure-material cells

Before the evolution, the per material and single-velocity mesh (SVM) mesh nodes at the interface are are all equal to each other and we denote this value x_i^n. After the evolution, the per material and SVM mesh nodes evolve to:

$$x_{i,mat_L}^{n+1} = \frac{\Delta t^2}{2} \frac{\phi_{i-1/2,mat_L} p_{i-1/2,mat_L}}{m_{i,mat_L}} + \Delta t \cdot u_{i,mat_L}^n \tag{39}$$

$$x_{i,mat_R}^{n+1} = \frac{\Delta t^2}{2} \frac{\phi_{i+1/2,mat_R} p_{i+1/2,mat_R}}{m_{i,mat_R}} + \Delta t \cdot u_{i,mat_R}^n \tag{40}$$

$$x_{i,SVM}^{n+1} = \frac{\Delta t^2}{2} \frac{\phi_{i-1/2,mat_L} p_{i-1/2,mat_L} - \phi_{i+1/2,mat_R} p_{i+1/2,mat_R}}{m_{i,mat_L} + m_{i,mat_R}} + \Delta t \cdot u_{i,SVM}^n \tag{41}$$

We would like to add a contact force $F_{i,mat}^C$ to the forces already applied to the individual-material nodes such that $x_{i,mat}^{n+1,C} = x_{i,SVM}^{n+1}$, where $x_{i,mat}^{n+1,C}$ is the position of node i for a material mat after contact forces have been applied, which would require:

$$x_{i,mat_L}^{n+1,C} = \frac{\Delta t^2}{2} \frac{\phi_{i-1/2,mat_L} p_{i-1/2,mat_L} + F_{i,mat_L}^C}{m_{i,mat_L}} + \Delta t \cdot u_{i,mat_L}^n = x_{i,SVM}^{n+1} \tag{42}$$

$$x_{i,mat_R}^{n+1,C} = \frac{\Delta t^2}{2} \frac{\phi_{i+1/2,mat_R} p_{i+1/2,mat_R} + F_{i,mat_R}^C}{m_{i,mat_R}} + \Delta t \cdot u_{i,mat_R}^n = x_{i,SVM}^{n+1} \tag{43}$$

Assuming a contact force of the form $F_{i,mat}^C = m_{i,mat}\alpha \cdot \theta_i$, that $\theta_i = x_{i,mat_L}^{n+1} - x_{i,mat_R}^{n+1}$, solving for the contact forces using 42 and 43 yields the following set of equations:

$$F_{i,mat_L}^C = \frac{-2}{\phi_{i-1,mat_L}} \frac{m_{i,mat_L} \cdot \theta_i}{\Delta t^2} \tag{44}$$

$$F_{i,mat_R}^C = \frac{2}{\phi_{i,mat_R}} \frac{m_{i,mat_R} \cdot \theta_{i-1}}{\Delta t^2} \tag{45}$$

These equations are a special case of the general forms of the contact forces (equations 37 and 38)

4.3.3 Telescoping Contact Forces

In order to ensure conservation of momentum when a contact force is applied on two materials, mat_L and mat_R, it is imperative that the total force on each material be equal and opposite.

For both the pure cell contact forces and the multi-material cell contact forces, it can be shown that in the formulations above the total force on the left material is always equal and opposite the total force on the right material

4.4 Remap

The per material mass, internal energy, and momentum are remapped from the per material meshes to a desired universal mesh after the corrector step in the algorithm. The per material meshes are the source mesh and the universal mesh is the target mesh. An exact intersection based remap is performed. To remap these conserved quantities, an cell-based intensive form of the quantity is first constructed. For the mass and internal energy, these quantities are simple to construct as they are just the material cell density $\rho_{i+1/2}$, and the material cell density times the specific internal energy $\rho_{i+1/2}\varepsilon_{i+1/2}$. The cell-based intensive momentum is more difficult to construct, since the velocities exist at cell nodes and not at cell centers. A zonal momentum for cell $\mathcal{C}_i$ is computed as

$$\mu_{i+1/2} = \frac{1}{2} M_{i+1/2}(u_i + u_{i+1}). \tag{46}$$

The intensive zonal momentum can then be calculated as

$$\tilde{\mu}_{i+1/2} = \frac{\mu_{i+1/2}}{V_{i+1/2}}. \tag{47}$$

The intensive zonal momentum can now be remapped using the same procedure as the density and intensive internal energy. After remapping the zonal momentum, it must be distributed to the nodes on the target mesh. This is done as

$$\mu_i = \frac{1}{2}\mu_{i-1/2} + \frac{1}{2}\mu_{i+1/2}. \tag{48}$$

The nodal velocity can then be obtained using the remapped nodal mass, m_i, as

$$u_i = \frac{\mu_i}{m_i}. \tag{49}$$

4.4.1 Kinetic Energy Fix

Ideally, all the quantities of interest (mass, momentum, internal energy, kinetic energy, total energy) are conserved through a remap. In reality, this is an over-constrained problem and we can only choose to conserve three of these. If mass and momentum are conservatively remapped to the target mesh, then the mass and velocity on the target mesh are defined. Since kinetic energy is only a function of mass and velocity, $KE = \frac{1}{2}mu^2$, its value on the target mesh

is already fixed. In general, the kinetic energy calculated from the remapped mass and velocity will differ from the kinetic energy on the source mesh. If total energy conservation is more important than internal energy conservation, a kinetic energy fix can be applied. This will result in conservation of total energy at the cost of internal and kinetic energy conservation.

Algorithm 2 Zonal Kinetic Energy Fix

1. Remap an intensive zonal kinetic energy conservatively
2. Compute zonal discrepancy between remapped kinetic energy and kinetic energy obtained from remapped mass and velocity
3. Add kinetic energy difference to the zone's internal energy

4.5 Void

Multi-velocity and remap allows us to solve problems that involve materials moving into and out of void. Void is a special material that represents a vacuum. It has zero mass, density, pressure, and specific internal energy and has no velocity. Therefore, it must be treated specially or else issues will arise with dividing by zero in the code. Materials can be initially separated by void and move through it, thus removing the void. Void can also be created when two stiffened gases separate from each other. In order to allow materials to move through void or create void as they separate, a remap procedure must be done. If the scheme were to stay purely Lagrangian, issues would potentially arise with cell volumes going to zero where void is present.

4.6 Closure Model for Multi-Material Cells

Within multi-material cells, the change in material properties must be determined. This is often done by specifying the relative compressibility of materials. In this work, the model of equal volumetric strain is used [1]. This enforces equal compressibility among materials within a cell, such that all materials change their volume by the same relative amount. In other words, a material's volume fraction remains constant. Other pressure closure models exist for multi-material cells, such as the model discussed in [3], that more accurately capture the interface physics between materials.

4.7 Updated Multi-Velocity Predictor-Corrector Method

The updated predictor-corrector scheme for multi-material, multi-velocity problems is as follows:

4.7.1 Predictor

Per Material Mesh Update

$$u_{i,mat}^{n+1,*} = u_{i,mat}^{n} - \frac{\Delta t}{m_{i,mat}}(\phi_{i+1/2,mat}^{n} \cdot p_{i+1/2,mat}^{n} - \phi_{i-1/2,mat}^{n} \cdot p_{i-1/2,mat}^{n}) \tag{50}$$

$$u_{i,mat}^{n+1/2,*} = \frac{1}{2}(u_{i,mat}^{n} + u_{i,mat}^{n+1,*}) \tag{51}$$

$$x_{i,mat}^{n+1,*} = x_{i,mat}^{n} + \Delta t u_{i,mat}^{n+1/2,*} \tag{52}$$

$$V_{i+1/2,mat}^{n+1,*} = x_{i+1,mat}^{n+1,*} - x_{i,mat}^{n+1,*} \tag{53}$$

$$\tag{54}$$

Single Velocity Mesh Update

$$u_{i,\text{SVM}}^{n+1,*} = u_{i,\text{SVM}}^{n} - \sum_{mat \in \mathcal{C}_i} \frac{\Delta t}{m_{i,mat}}(\phi_{i+1/2,mat}^{n} \cdot p_{i+1/2,mat}^{n} - \phi_{i-1/2,mat}^{n} \cdot p_{i-1/2,mat}^{n}) \tag{55}$$

$$u_{i,\text{SVM}}^{n+1/2,*} = \frac{1}{2}(u_{i,\text{SVM}}^{n} + u_{i,\text{SVM}}^{n+1,*}) \tag{56}$$

$$x_{i,\text{SVM}}^{n+1,*} = x_{i,\text{SVM}}^{n} + \Delta t u_{i,\text{SVM}}^{n+1/2,*} \tag{57}$$

$$V_{i+1/2,\text{SVM}}^{n+1,*} = x_{i+1,\text{SVM}}^{n+1,*} - x_{i,\text{SVM}}^{n+1,*} \tag{58}$$

$$\tag{59}$$

After evolving the per material meshes and the single velocity mesh, the material polygons from the per material meshes are remapped into the single velocity mesh. The overfill is then computed on the single velocity mesh using equation 22 and the contact forces are computed using equations 37-38 or **??-??** depending on whether the cells are pure or multi-material.

Re-Evolution of Per Material Meshes

$$u_{i,mat}^{n+1,*} = u_{i,mat}^{n} - \frac{\Delta t}{m_{i,mat}}(\phi_{i+1/2,mat}^{n} \cdot p_{i+1/2,mat}^{n} - \phi_{i-1/2,mat}^{n} \cdot p_{i-1/2,mat}^{n} - F_{i,mat}^{C}) \tag{60}$$

$$u_{i,mat}^{n+1/2,*} = \frac{1}{2}(u_{i,mat}^{n} + u_{i,mat}^{n+1,*}) \tag{61}$$

$$x_{i,mat}^{n+1,*} = x_{i,mat}^{n} + \Delta t u_{i,mat}^{n+1/2,*} \tag{62}$$

$$V_{i+1/2,mat}^{n+1,*} = x_{i+1,mat}^{n+1,*} - x_{i,mat}^{n+1,*} \tag{63}$$

$$\tag{64}$$

Evolution of Thermodynamic Variables

$$\tau^{n+1,*}_{i+1/2,mat} = \phi^{n}_{i+1/2,mat} \cdot V^{n+1,*}_{i+1/2,mat} / M_{i+1/2,mat} \tag{65}$$

$$\begin{aligned}\varepsilon^{n+1,*}_{i+1/2,mat} = \varepsilon^{n}_{i+1/2,mat} - \\ \frac{\Delta t}{M_{i+1/2,mat}} \Bigg[\phi^{n}_{i+1/2,mat} \cdot p^{n}_{i+1/2,mat} (u^{n+1/2,*}_{i+1,mat} - u^{n+1/2,*}_{i,mat}) + \\ \frac{1}{2} \sum_{\text{mat} \in \mathcal{C}_\text{i}} (F^{C}_{i,mat} \cdot u^{n+1/2,*}_{i,mat} + F^{C}_{i+1,mat} \cdot u^{n+1/2,*}_{i+1,mat}) \Bigg]\end{aligned} \tag{66}$$

$$p^{n+1,*}_{i+1/2,mat} = \mathcal{P}(\tau^{n+1,*}_{i+1/2,mat}, \varepsilon^{n+1,*}_{i+1/2,mat}) \tag{67}$$

4.7.2 Corrector

The corrector step is similar to the predictor step, with the exception of an optional remap of quantities to a desired universal mesh at the end of the timestep.

Per Material Mesh Update

$$\begin{aligned}u^{n+1}_{i,mat} = u^{n}_{i,mat} - \frac{1}{2} \frac{\Delta t}{m_{i,mat}} \big(\phi^{n}_{i+1/2,mat} \cdot [p^{n}_{i+1/2,mat} + p^{n+1,*}_{i+1/2,mat}] - \\ \phi^{n}_{i+1/2,mat} \cdot [p^{n}_{i-1/2,mat} + p^{n+1,*}_{i-1/2,mat}] \big)\end{aligned} \tag{68}$$

$$u^{n+1/2}_{i,mat} = \frac{1}{2}(u^{n}_{i,mat} + u^{n+1}_{i,mat}) \tag{69}$$

$$x^{n+1}_{i,mat} = x^{n}_{i,mat} + \Delta t u^{n+1/2}_{i,mat} \tag{70}$$

$$V^{n+1}_{i+1/2,mat} = x^{n+1}_{i+1,mat} - x^{n+1}_{i,mat} \tag{71}$$

$$\tag{72}$$

Single Velocity Mesh Update

$$\begin{aligned}u^{n+1}_{i,\text{SVM}} = u^{n}_{i,\text{SVM}} - \frac{1}{2} \sum_{mat \in \mathcal{C}_i} \frac{\Delta t}{m_{i,mat}} \big(\phi^{n}_{i+1/2,mat} \cdot [p^{n}_{i+1/2,mat} + p^{n+1,*}_{i+1/2,mat}] - \\ \phi^{n}_{i+1/2,mat} \cdot [p^{n}_{i-1/2,mat} + p^{n+1,*}_{i-1/2,mat}] \big)\end{aligned} \tag{73}$$

$$u^{n+1/2}_{i,\text{SVM}} = \frac{1}{2}(u^{n}_{i,\text{SVM}} + u^{n+1}_{i,\text{SVM}}) \tag{74}$$

$$x^{n+1}_{i,\text{SVM}} = x^{n}_{i,\text{SVM}} + \Delta t u^{n+1/2}_{i,\text{SVM}} \tag{75}$$

$$V^{n+1}_{i+1/2,\text{SVM}} = x^{n+1}_{i+1,\text{SVM}} - x^{n+1}_{i,\text{SVM}} \tag{76}$$

After evolving the per material meshes and the single velocity mesh, the material polygons from the per material meshes are remapped into the single velocity mesh. The overfill is then computed on the single velocity mesh using equation 22 and the contact forces are computed using equations 37-38 or **??**-**??** depending on whether the cells are pure or multi-material. This is the same procedure as used in the predictor step.

Re-Evolution of Per Material Meshes

$$u_{i,mat}^{n+1} = u_{i,mat}^{n} - \frac{\Delta t}{m_{i,mat}}\Big(\frac{1}{2}\phi_{i+1/2,mat}^{n} \cdot [p_{i+1/2,mat}^{n} + p_{i+1/2,mat}^{n+1,*}] - \frac{1}{2}\phi_{i+1/2,mat}^{n} \cdot [p_{i-1/2,mat}^{n} + p_{i-1/2,mat}^{n+1,*}] - F_{i,mat}^{C}\Big) \tag{77}$$

$$u_{i,mat}^{n+1/2} = \frac{1}{2}(u_{i,mat}^{n} + u_{i,mat}^{n+1}) \tag{78}$$

$$x_{i,mat}^{n+1} = x_{i,mat}^{n} + \Delta t u_{i,mat}^{n+1/2} \tag{79}$$

$$V_{i+1/2,mat}^{n+1} = x_{i+1,mat}^{n+1} - x_{i,mat}^{n+1} \tag{80}$$

$$\tag{81}$$

Evolution of Thermodynamic Variables

$$\tau_{i+1/2,mat}^{n+1} = \phi_{i+1/2,mat}^{n} \cdot V_{i+1/2,mat}^{n+1} / M_{i+1/2,mat} \tag{82}$$

$$\varepsilon_{i+1/2,mat}^{n+1} = \varepsilon_{i+1/2,mat}^{n} - \frac{\Delta t}{M_{i+1/2,mat}}\left[\frac{1}{2}\phi_{i+1/2,mat}^{n} \cdot (p_{i+1/2,mat}^{n} + p_{i+1/2,mat}^{n+1,*})(u_{i+1,mat}^{n+1/2} - u_{i,mat}^{n+1/2}) + \frac{1}{2}\sum_{mat \in \mathcal{C}_i}(F_{i,mat}^{C} \cdot u_{i,mat}^{n+1/2} + F_{i+1,mat}^{C} \cdot u_{i+1,mat}^{n+1/2})\right] \tag{83}$$

$$p_{i+1/2,mat}^{n+1} = \mathcal{P}(\tau_{i+1/2,mat}^{n+1}, \varepsilon_{i+1/2,mat}^{n+1}) \tag{84}$$

$$\tag{85}$$

In the corrector step, there exists the option to remap the material quantities to a new universal mesh. For problems with void present, this remap step is mandatory.

5 Results

5.1 Modified Sod Shock Tube

We consider the modified Sod shock tube problem proposed by Shashkov in [5], with initial conditions

$$(\gamma, \rho, \varepsilon, p, u) = \begin{cases} (2, \quad 1, \quad\quad 2, \; 2, \quad 0) & \text{if } 0 \le x \le 0.5 \\ (1.4, \; 0.125, \; 2, \; 0.1, \; 0) & \text{if } 0.5 < x \le 1 \end{cases} \tag{86}$$

and a final time of $t_{\text{final}} = 0.2$s. An analytic solution can be obtained through solving the corresponding Riemann problem. Since this is a true multi-material problem with an analytic solution available, this problem is used to test all the components of our multi-velocity solution algorithm both independently and

together. Figures 3-6 show the comparison of the numerical and analytical solution at time $t = 2$s for the single velocity case, the single velocity with remap case, the multi-velocity case, and the multi-velocity with remap case for $N_x = 1000$ cells.

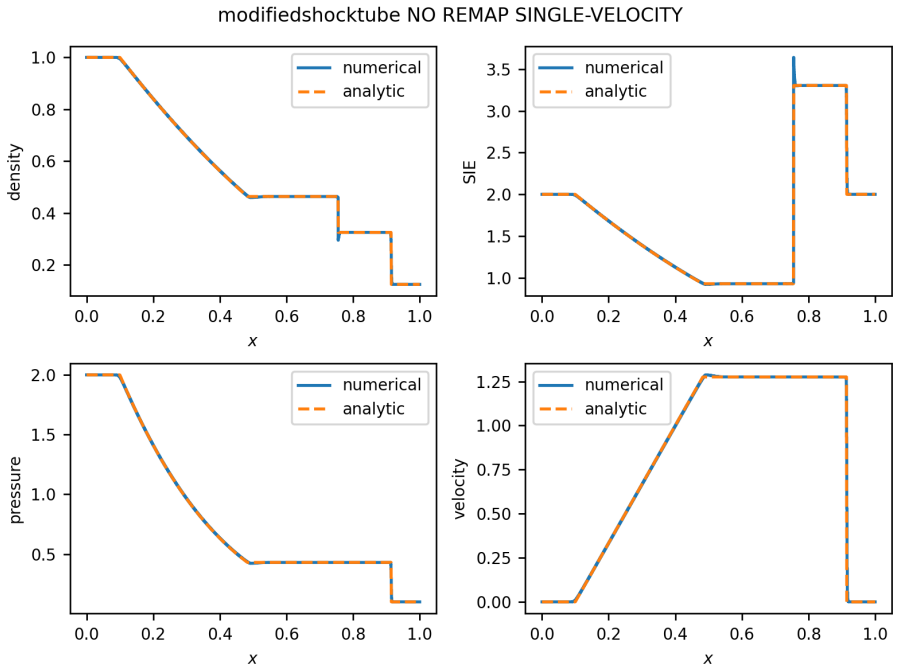

Figure 3: Numerical vs analytical solutions of the modified sod shock tube problem using standard SGH with no remap step.

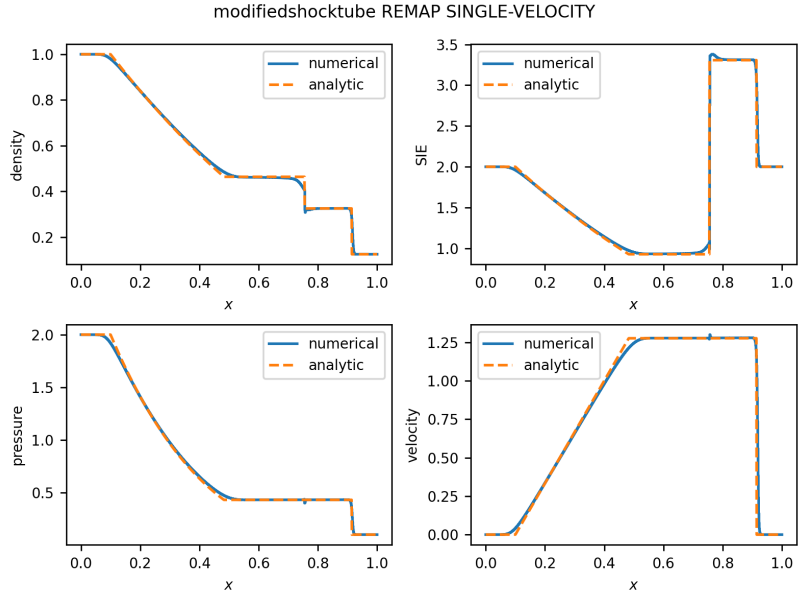

Figure 4: Numerical vs analytical solutions of the modified sod shock tube problem using standard SGH with a remap step.

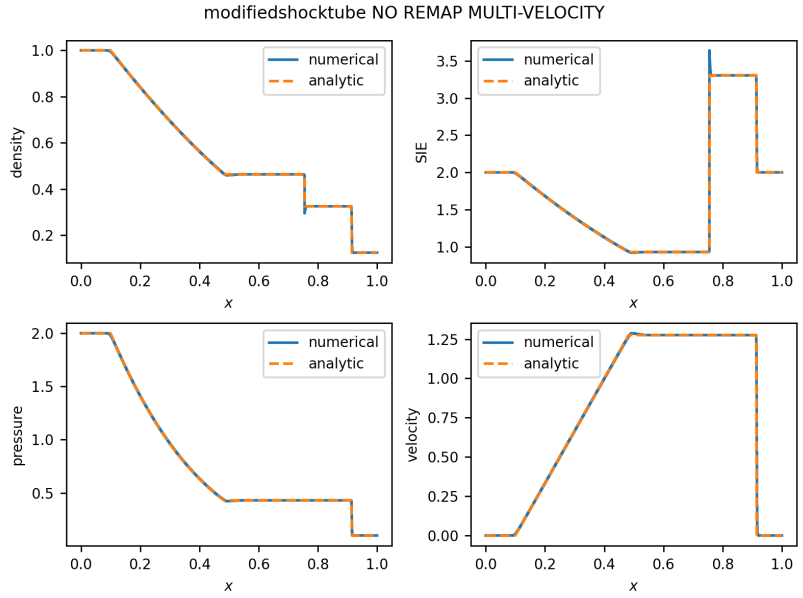

Figure 5: Numerical vs analytical solutions of the modified sod shock tube problem using the new multi-velocity scheme with no remap step.

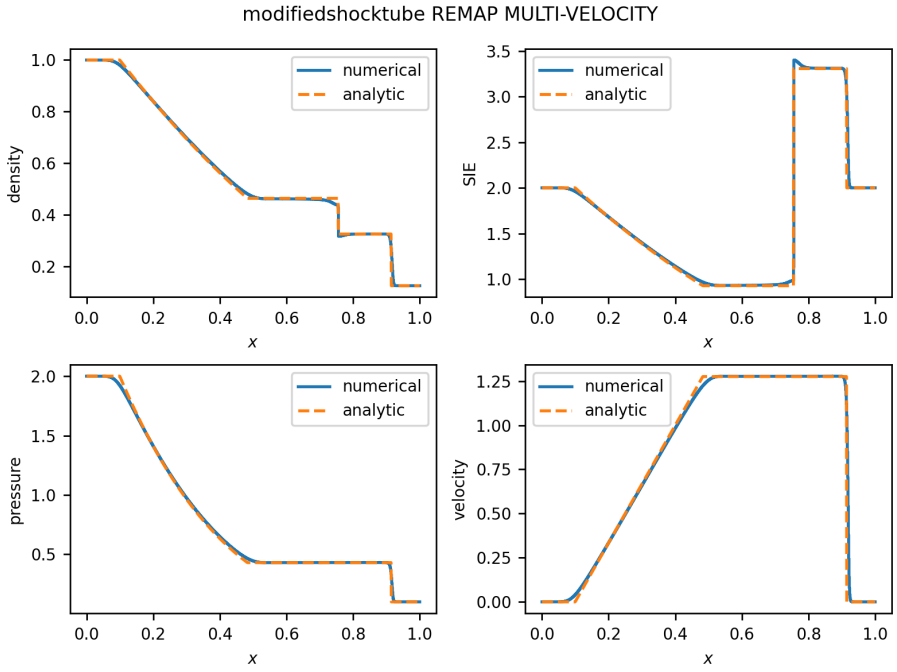

Figure 6: Numerical vs analytical solutions of the modified sod shock tube problem using the new multi-velocity scheme with a remap step.

These comparisons show that all components of our solution method work as expected and converge to the analytic solution. Furthermore, we have shown that the multi-velocity scheme properly replicates the correct behavior of standard SGH.

5.2 Stiff Gas Collision

A stiff gas collision test case was devised that allows us to test our contact forces, void closure, and void opening. In this problem, two identical stiffened gas "blocks" are separated by void. The blocks have initial velocities pointing towards each other. The blocks will move through the void, come into contact, and then separate after pressure waves move through them. As the blocks begin to separate, void will form in the space between them. The problem should ideally remain symmetric at all times as both blocks have the same initial states and equal and opposite velocities. The initial conditions are

$$(\gamma, \rho, p, u, p_\infty) = \begin{cases} (4.4,\ 2,\ 0,\ \ 5,\ 1) & \text{if } 0 \leq x \leq 0.25 \\ (4.4,\ 2,\ 0, -5,\ 1) & \text{if } 0.75 \leq x \leq 1 \\ \text{void} & \text{else} \end{cases} \tag{87}$$

and the final time is $t_{\text{final}} = 1.0$s.

Figures 7-9 show the initial condition, the solution at the time of first contact, the solution slightly after first contact, and the solution after the materials have separated. As can be seen in the figures the solution remains symmetric and qualitatively behaves as expected.

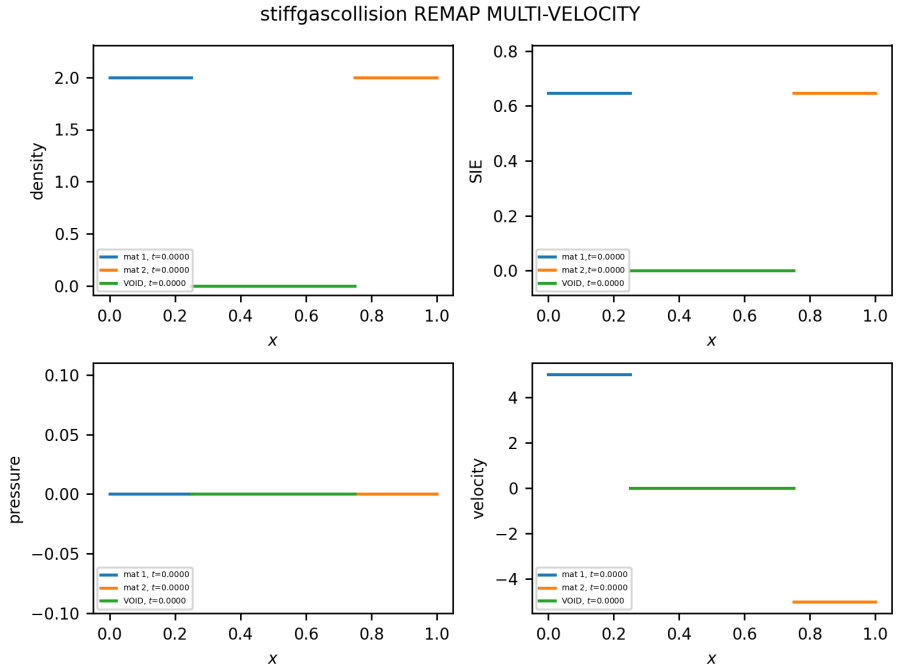

Figure 7: Initial condition for the stiff gas collision problem.

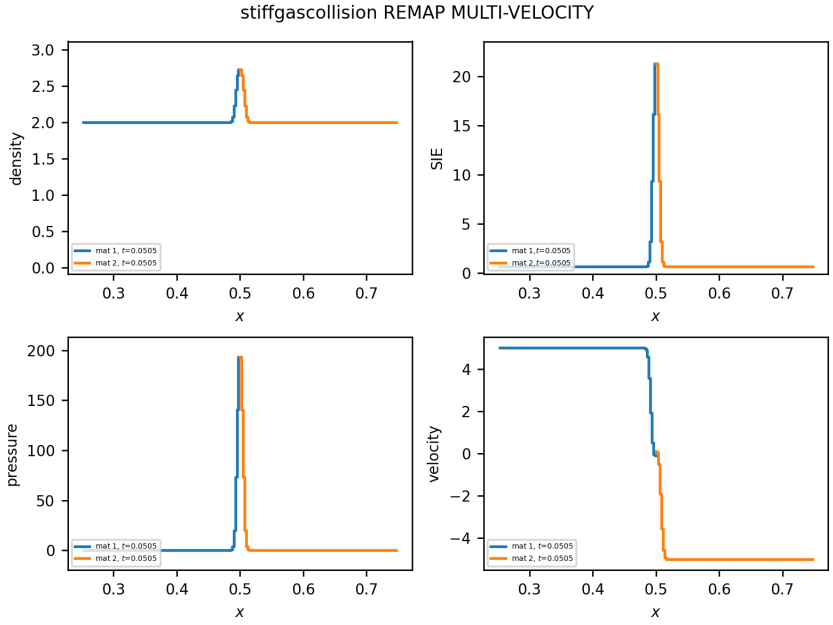

Figure 8: First impact between materials for the stiff gas collision problem.

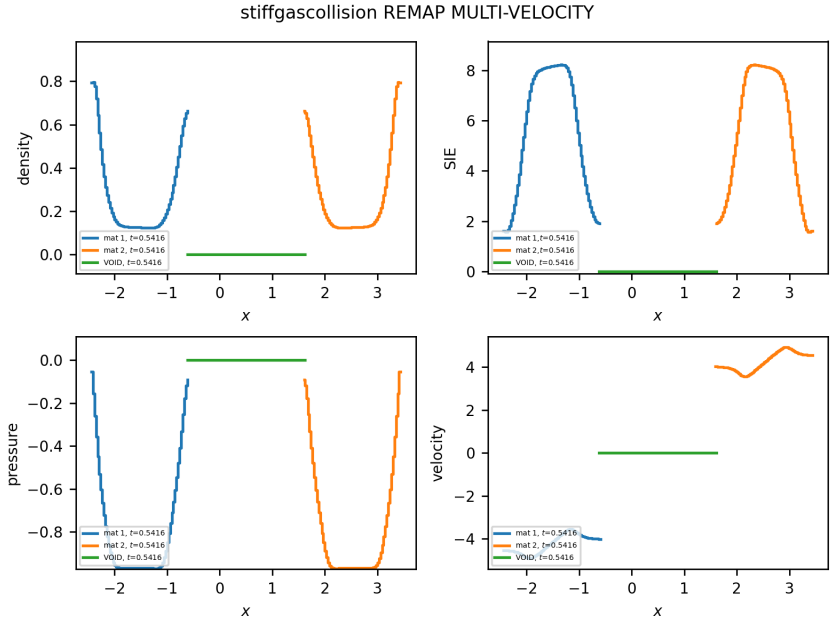

Figure 9: Separation of the two materials after collision.

5.3 Stiff Gas Separation: Multi vs Single Velocity

In order to demonstrate the advantages of the multi-velocity method as opposed to single-velocity ALE, we demonstrate a stiff gas separation case. In this problem, two identical stiffened gas "blocks" are adjacent to each other, with velocities equal in magnitude pointing away from one another. The expected behavior is that the blocks immediately, cleanly, and symmetrically separate from each other. To demonstrate the advantage of multi-velocity, this case is tested with both multi-velocity and single velocity ALE. The initial conditions are

$$(\gamma, \rho, p, u, p_\infty) = \begin{cases} (4.4,\ 2,\ 0,\ \ 5,\ 1) & \text{if } 0 \leq x \leq 0.5 \\ (4.4,\ 2,\ 0, -5,\ 1) & \text{if } 0.5 < x \leq 1 \end{cases} \tag{88}$$

and the final time is $t_{\text{final}} = 0.0010$s.

Figure 10 shows the initial conditions, figure 11 shows the evolution of the system after 0.0010s for the multi-velocity method, and figure 12 shows the evolution of the system after 0.0010s for the single-velocity method. As can be seen in figure 11, the multi-velocity ALE method allows the two stiffened gasses to separate from each other and is able to inject void, as is qualitatively expected. In figure 12, the single-velocity ALE method fails to allow the materials to separate, as the interface node shares a velocity between materials.

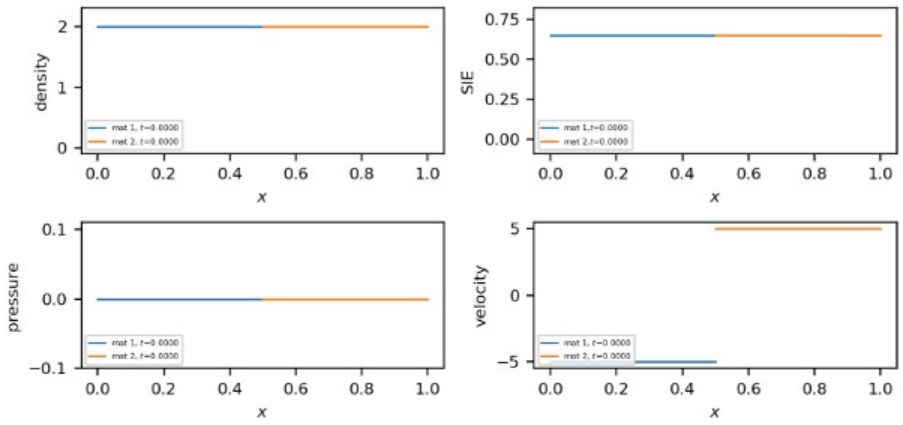

Figure 10: Initial condition for Stiff Gas Separation problem.

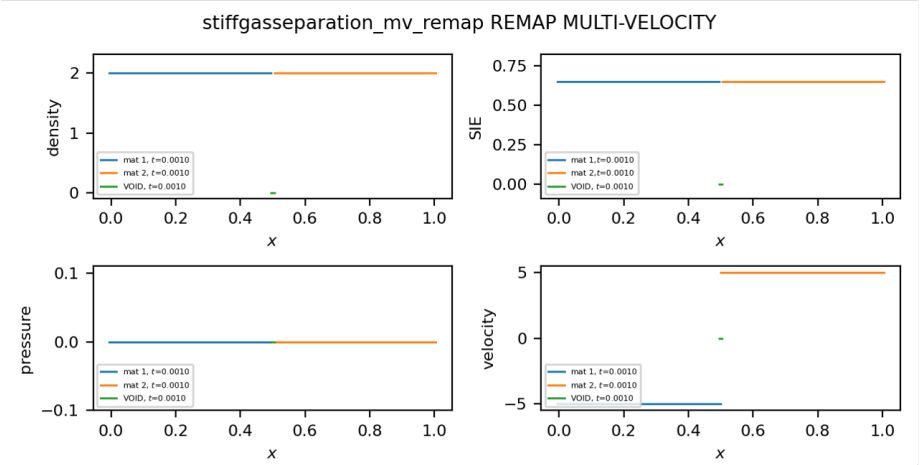

Figure 11: 0.0010s of evolution for the stiff gas separation problem using the multi-velocity method

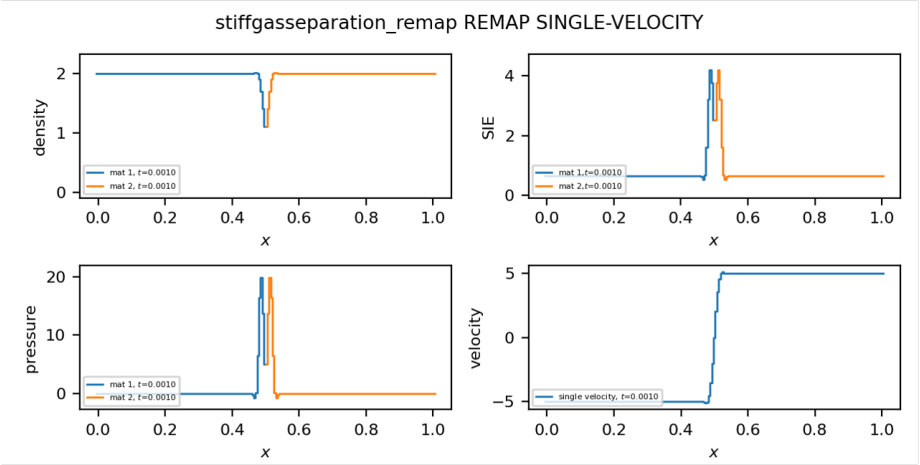

Figure 12: 0.0010s of evolution for the stiff gas separation problem using the single-velocity method

5.4 Sedov-Like Explosion Wave with Flyer Plates

To test the robustness of our algorithm and simulate a potential problem of interest, we consider the Sedov-like explosion wave problem described in [6]. For this problem, there is a region of ideal gas in the left of the domain, with a point explosion in the first computational cell, and a system of flyer plates separated by vacuum to the right. The initial conditions are

$$(\gamma, \rho, \varepsilon, p, u, p_\infty) = \begin{cases} (\frac{5}{3}, \ 1, \ 100, \ \ 66.7, \ \ \ \ 0, \ 0) & \text{in first cell} \\ (\frac{5}{3}, \ 1, \ 1\text{E}{-9}, \ 6.7\text{E}{-10}, \ 0, \ 0) & \text{if } -4 \leq x \leq 1 \\ (4.4, \ 2, \ 0.647, \ 0, \ \ \ \ \ \ 0, \ 1) & \text{if } -1 < x \leq 0.5, \ 0.5 < x \leq 1, \ 2 < x \leq 2.5 \\ \text{void} & \text{else} \end{cases} \tag{89}$$

and the final time is $t_{\text{final}} = 12\text{s}$. The solution to this problem at various key timesteps is shown in figures 13-19. Contact between the initial pressure wave from the explosion and the flyer plates can be seen. Multiple material contacts and void closures and openings can be seen as well.

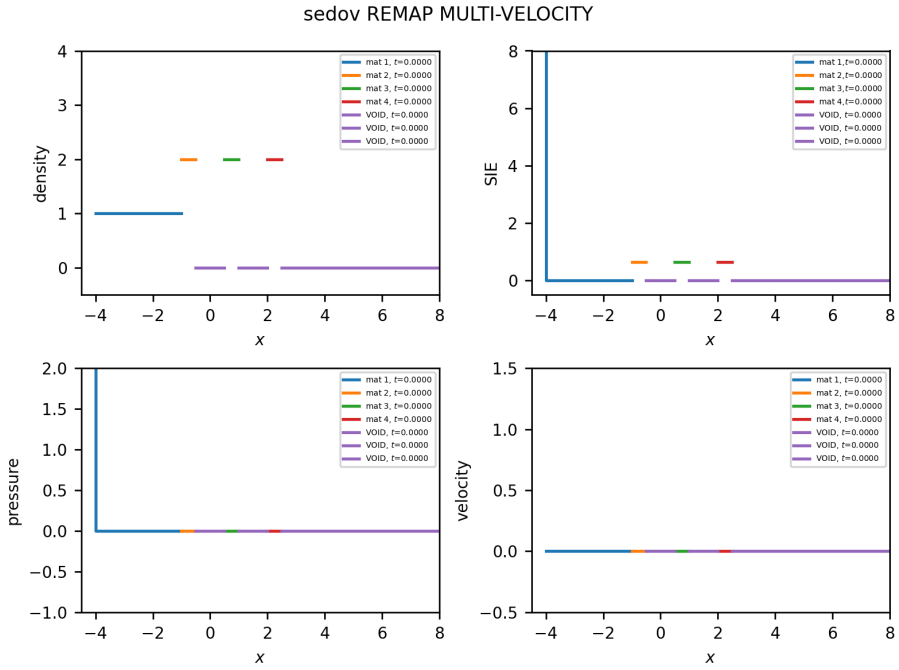

Figure 13: Initial condition for Sedov problem.

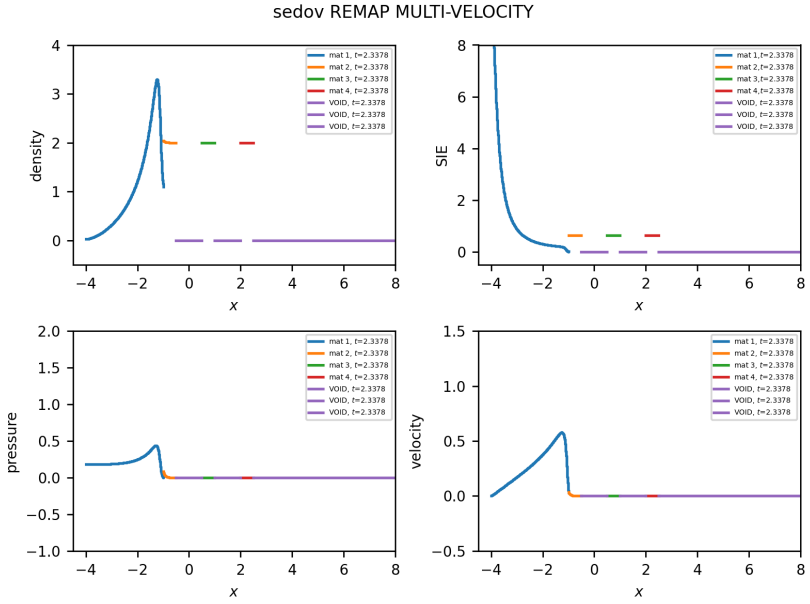

Figure 14: First contact between the pressure wave in the ideal gas and the leftmost flyer plate.

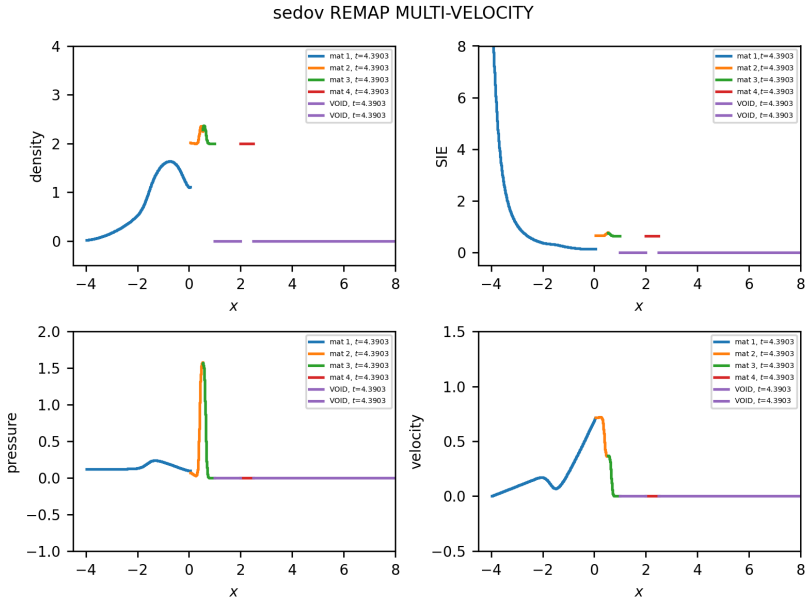

Figure 15: First contact between the first and second flyer plates.

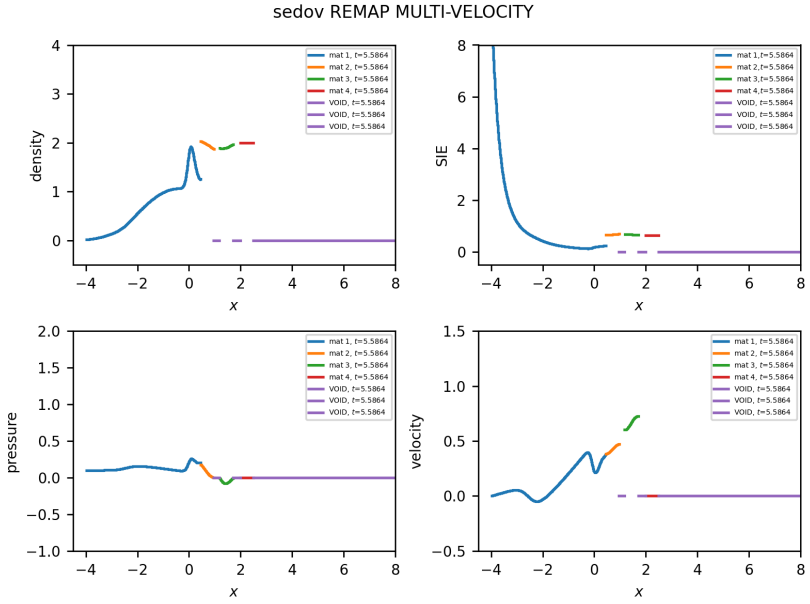

Figure 16: Reopening of void between first and second flyer plates.

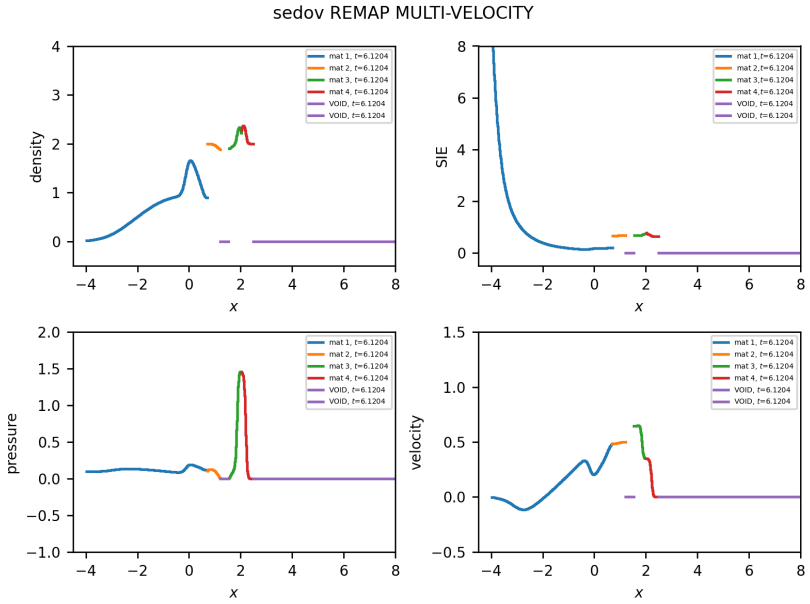

Figure 17: First contact between second and third flyer plates.

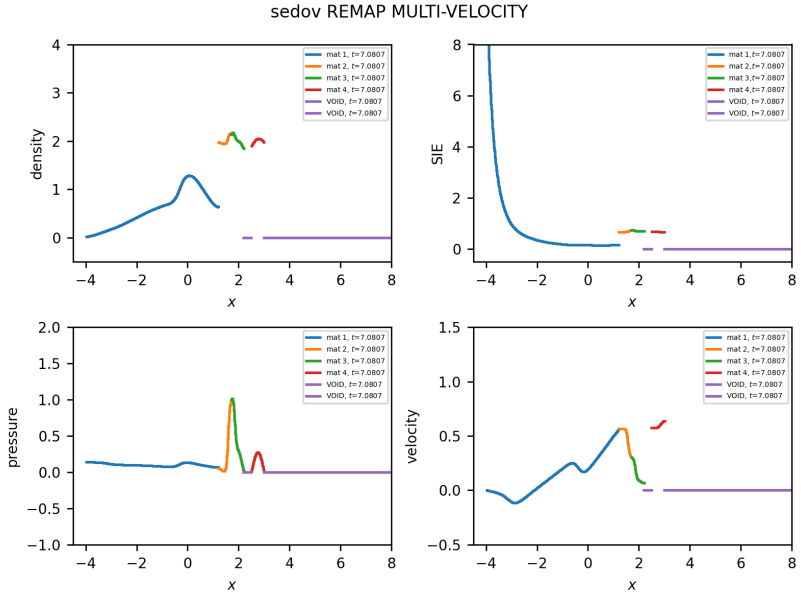

Figure 18: Second contact between first and second flyer plates, and void opening between second and third flyer plates.

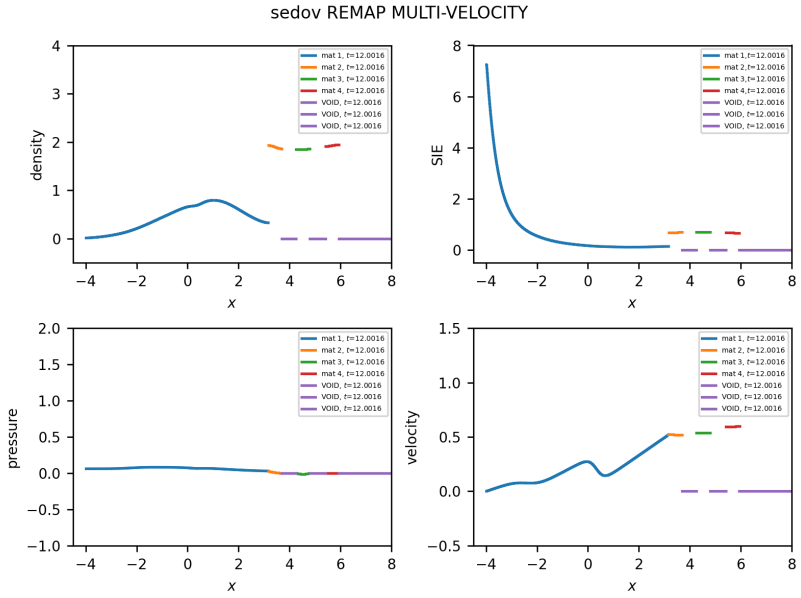

Figure 19: Final condition for Sedov problem. The flyer plates have separated and void spaces have opened between them.

6 Summary and Conclusions

We have developed a one-dimensional Arbitrary Lagrangian-Eulerian (ALE) hydrodynamics code with Multi-Velocity capabilities that can successfully assign materials their own individual velocities, as opposed to previous ALE methods where all materials share a single velocity. Our multi-velocity method is able to properly simulate one-dimensional contact mechanics, namely materials being able to come into contact and separate from one-another, as opposed to single-velocity ALE methods which cannot simulate material separation.

This is made possible by the application of a contact force to individual materials when overfill occurs, which is derived such that material-wise positions and velocities match exactly. We consider a Staggered-Grid Hydrodynamics (SGH) formulation and evolve thermodynamic quantities in a Lagrangian timestep using a discretized predictor-corrector scheme, which is optionally followed by a remap to a universal mesh. This remapping to a universal mesh, which we choose to be an equidistant set of points along the problem domain, is necessary in situations where void must be injected or removed. We test our method on a variety of test cases, showcasing how the results of our method converges to analytical results, when available, and qualitatively matches expected behaviors while conserving total energy.

While total energy is conserved by our method, both within the Lagrangian timestep and the remapping procedure, it is important to note that not all quantities are conserved by the remapping procedure. An ideal remapping procedure conserves mass, momentum, internal energy, kinetic energy, and total energy, however, in-reality this is an over-constrained problem. While we cannot conserve all five of these quantities, we can choose to conserve three of them (namely mass, momentum, and total energy), through the usage of a kinetic energy fix procedure.

While our work is able to allow for multi-velocity and contact mechanic capabilities in one-dimensional ALE hydrodynamics, further work is required to expand this work to allow for multi-velocity hydrodynamics in two and three dimensions. We suspect that the derivation of a contact force is much more complicated in higher dimensions, and that it may not necessarily be able to be computed in only one 'pass'. In two and three dimensions, much more interesting contact mechanics behaviors, namely tangential sliding, can be simulated. This is necessary for the integration of contact mechanics capabilities within ALE-based multiphysics codes.

References

[1] D. J. Benson. Computational methods in lagrangian and eulerian hydrocodes. *Computer Methods in Applied Mechanics and Engineering*, 99(2-3):235–394, 1992.

[2] E. Caramana, D. Burton, M. Shashkov, and P. Whalen. The construction of compatible hydrodynamics algorithms utilizing conservation of total energy. *Journal of Computational Physics*, 146(1):227–262, 1998.

[3] J. Kamm and M. Shashkov. A pressure relaxation closure model for one-dimensional, two-material lagrangian hydrodynamics based on the riemann problem. *Communications in Computational Physics*, LA-UR-09-00659, 2010.

[4] M. Kenamond, D. Kuzmin, and M. Shashkov. Intersection-distribution-based remapping between arbitrary meshes for staggered multi-material arbitrary lagrangian-eulerian hydrodynamics. *Journal of Compuational Physics*, 429:110014, 2021.

[5] M. Shashkov. Closure models for multimaterial cells in arbitrary lagrangian-eulerian hydrocodes. *International Journal for Numerical Methods in Fluids*, 56(8):1497–1504, 2007.

[6] M. Shashkov. Algorithms for improved solution robustness, accuracy mesh adaptivity. In *Proceedings of JOWOG-42*, LA-UR-15-23913, United Kingdom, 2015.

[7] N. Vaughn-Kukura, M. Buechler, M. Kenamond, and M. Shashkov. Overset mesh method for arbitrary lagrangian eulerian contact on unstructures general polyhedral meshes. *Proceedings of the 17th Hypervelocity Impact Symposium*, 2024.

[8] J. von Neumann and R. Richtmyer. A method for the numerical calculation of hydrodynamic shocks. *Journal of Applied Physics*, 21(3):232–237, 1950.

Appendix A: Energy Conservation

For total energy conservation, we require that $\Delta KE = -\Delta IE$. For a material mat and point p the momentum equation update can be written as

$$m_{p,mat}\frac{u_{p,mat}^{n+1} - u_{p,mat}^{n}}{\Delta t} = \sum_{z \in Z(p)} (F_{p,mat})_{zp}^{n} \tag{90}$$

where $(F_{p,mat})_{zp}^{n}$ is the sub-zonal material corner force. The half timestep velocity is defined as

$$u_{p,mat}^{n+1/2} = \frac{u_{p,mat}^{n} + u_{p,mat}^{n+1}}{2}. \tag{91}$$

Multiplying through the momentum equation

$$\begin{aligned}
\sum_{p} m_{p,mat}\frac{(u_{p,mat}^{n+1})^2 - (u_{p,mat}^{n})^2}{\Delta t} &= \sum_{p}\sum_{z \in Z(p)} (F_{p,mat})_{zp}^{n} u_{p,mat}^{n+1/2} \\
\Delta KE_{mat} &= \sum_{p}\sum_{z \in Z(p)} (F_{p,mat})_{zp}^{n} u_{p,mat}^{n+1/2} \\
-\Delta IE_{mat} &= \sum_{p}\sum_{z \in Z(p)} (F_{p,mat})_{zp}^{n} u_{p,mat}^{n+1/2} \\
-\sum_{z} m_{z,mat}\frac{\varepsilon_{z,mat}^{n+1} - \varepsilon_{z,mat}^{n}}{\Delta t} &= \sum_{z}\sum_{p \in P(z)} (F_{p,mat})_{zp}^{n} u_{p,mat}^{n+1/2}
\end{aligned} \tag{92}$$

The internal energy update for each material in a given zone is

$$m_{z,mat}\frac{\varepsilon_{z,mat}^{n+1} - \varepsilon_{z,mat}^{n}}{\Delta t} = -\sum_{p \in P(z)} (F_{p,mat})_{zp}^{n} u_{p,mat}^{n+1/2}. \tag{93}$$

For standard SGH, this reduces to

$$m_{z,mat}\frac{\varepsilon_{z,mat}^{n+1} - \varepsilon_{z,mat}^{n}}{\Delta t} = -\phi_{z,mat} p_{z,mat} \sum_{p \in P(z)} u_{p,mat}^{n+1/2} S_{zp}^{n} \tag{94}$$

where S_{zp}^{n} is a direction vector pointing from the cell center to the point in 1D.

For multi-velocity with contact forces, equation 93 is modified to allow for total energy exchange between materials. If we enforce that $\Delta KE_{mat} = -\Delta IE_{mat}$ for each material, this will by construction result in the total energy of each material remaining constant throughout the simulation. In some cases, this is correct behavior, but in general materials will exchange energy and the per material total energy will change over time. One such example is a standard shock tube problem. In a shock tube problem, the material in the driver section initially has more total energy than the material in the driven section. As

time passes, the driver section material will lose some of its total energy as it is exchanged with the material in the driven section. For multi-velocity total energy conservation, it is instead necessary to enforce that

$$\sum_{mat}^{N_{mat}} \Delta KE_{mat} = -\sum_{mat}^{N_{mat}} \Delta IE_{mat}, \tag{95}$$

the total change in kinetic energy over all materials must equal the total change in internal energy over all materials. The change in kinetic energy for a material in a multi-velocity system can be written as

$$\Delta KE_{mat} = \sum_{z} \sum_{p \in P(z)} (\phi_{z,mat} p_{z,mat} S^{n}_{zp} + F^{C}_{p,mat}) u^{n+1/2}_{p,mat} \tag{96}$$

which gives the change in kinetic energy due to contact forces for a material as

$$\Delta KE^{C}_{mat} = \sum_{z} \sum_{p \in P(z)} F^{C}_{p,mat} u^{n+1/2}_{p,mat}. \tag{97}$$

The multi-velocity internal energy update including contact forces is listed in equations 66 and 83. This formulation has been tested and verified to work for two materials with arbitrary volume fraction.

Appendix B: Notes on the Remap

There are many potential ways of remapping the nodal velocity and performing the kinetic energy fix. We found the most success in doing a cell based velocity remap (as described in §4.4). We also found the most success using a cell based kinetic energy fix for the single velocity case and a node based kinetic energy fix for the multi-velocity case. The algorithm for the node based kinetic energy fix was inspired by [4]. In this, a nodal kinetic energy obtained from the conservatively remapped kinetic energy and another nodal kinetic energy obtained from the remapped velocity are constructed. The nodal difference between the conservatively remapped kinetic energy and kinetic energy obtained from remapped velocity is then added to the internal energy of neighboring cells based on a weighting of their specific internal energies. This led to a more accurate distribution of energy between cells. We found that when we did a simple cell based kinetic energy fix for the multi-velocity case, it would occasionally lead to artificially low and high regions of specific internal energy, while still conserving the total energy.

Appendix C: Pure Cell Contact Force Derivation

The pure cell contact force equations (Equations 42 and 43) can be shown to be derived from the general form of a contact force (Equation 37) as follows. Consider the general form of a contact force

$$F^C_{i,mat} = \frac{m_{i,mat}F_{i,SVM}}{\sum_{mat} m_{i,mat}} + \frac{2}{\Delta t} m_{i,mat}(u^n_{i,SVM} - u^n_{i,mat}) - F_{i,mat} \tag{98}$$

In the pure cell case, we can assume that $u^n_{i,SVM} = u^n_{i,mat}$. It is known that $F_{i,SVM} = \phi_{i-1/2,mat_L} p_{i-1/2,mat_L} - \phi_{i+1/2,mat_R} p_{i+1/2,mat_R}$. Let us consider solving for the contact force for material mat_L, which means that $F_{i,mat} = \phi_{i-1/2,mat_L} p_{i-1/2,mat_L}$, which yields:

$$\begin{aligned} F^C_{i,mat_L} = & \frac{m_{i,mat_L}(\phi_{i-1/2,mat_L} p_{i-1/2,mat_L} - \phi_{i+1/2,mat_R} p_{i+1/2,mat_R})}{m_{i,mat_L} + m_{i,mat_R}} \\ & - \phi_{i-1/2,mat_L} p_{i-1/2,mat_L} \end{aligned} \tag{99}$$

$$\begin{aligned} \Rightarrow F^C_{i,mat_L} = & [m_{i,mat_L}(\phi_{i-1/2,mat_L} p_{i-1/2,mat_L} - \phi_{i+1/2,mat_R} p_{i+1/2,mat_R}) \\ & - \phi_{i-1/2,mat_L} p_{i-1/2,mat_L}(m_{i,mat_L} + m_{i,mat_R})]/(m_{i,mat_L} + m_{i,mat_R}) \end{aligned} \tag{100}$$

$$\Rightarrow F^C_{i,mat_L} = \frac{-\phi_{i+1/2,mat_R} p_{i+1/2,mat_R} m_{i,mat_L} - \phi_{i-1/2,mat_L} p_{i-1/2,mat_L} m_{i,mat_R}}{m_{i,mat_L} + m_{i,mat_R}} \tag{101}$$

For the left material, the overfill is given by

$$\theta_{mat_L} = x^{n+1}_{i,mat_L} - x^{n+1}_{i,SVM} \tag{102}$$

Which is equivalent to

$$\begin{aligned} \theta_{mat_L} = & \phi_{i-1/2,mat_L} \frac{\Delta t^2}{2} \Big(\frac{\phi_{i-1/2,mat_L} p_{i-1/2,mat_L}}{m_{i,mat_L}} \\ & - \frac{\phi_{i-1/2,mat_L} p_{i-1/2,mat_L} - \phi_{i+1/2,mat_R} p_{i+1/2,mat_R}}{m_{i,matL} + m_{i,matR}} \Big) \end{aligned} \tag{103}$$

$$\begin{aligned} \Rightarrow \theta_{mat_L} = & [\phi_{i-1/2,mat_L} \frac{\Delta t^2}{2} (\phi_{i-1/2,mat_L} p_{i-1/2,mat_L}(m_{i,matL} + m_{i,matR}) \\ & - m_{i,mat_L}(\phi_{i-1/2,mat_L} p_{i-1/2,mat_L} - \phi_{i+1/2,mat_R} p_{i+1/2,mat_R})] \\ & /(m_{i,mat_L}(m_{i,mat_L} + m_{i,mat_R})) \end{aligned} \tag{104}$$

$$\begin{aligned} \Rightarrow \theta_{mat_L} = & \phi_{i-1/2,mat_L} \frac{\Delta t^2}{2} [\phi_{i+1/2,mat_R} p_{i+1/2,mat_R} m_{i,mat_L} \\ & + \phi_{i-1/2,mat_L} p_{i-1/2,mat_L} m_{i,mat_R}] / m_{i,mat_L}(m_{i,mat_L} + m_{i,mat_R}) \end{aligned} \tag{105}$$

From this point, we find that multiplying θ_{mat_L} by $\frac{-2*m_{i,mat_L}}{\phi_{i-1/2,mat_L}\Delta t^2}$ yields

$$\frac{-2 * m_{i,mat_L}\theta_{mat_L}}{\phi_{i-1/2,mat_L}\Delta t^2} = \frac{-\phi_{i+1/2,mat_R}p_{i+1/2,mat_R}m_{i,mat_L} - \phi_{i-1/2,mat_L}p_{i-1/2,mat_L}m_{i,mat_R}}{m_{i,mat_L} + m_{i,mat_R}} \tag{106}$$

Which is equivalent to Equation 101, from which we arrive to the pure cell contact force for mat_L:

$$F^C_{i,mat_L} = \frac{-2 * m_{i,mat_L}\theta_{mat_L}}{\phi_{i-1/2,mat_L}\Delta t^2} \tag{107}$$

As was show in equation 44. A similar approach can be used to prove the validity of equation 45, the pure cell contact force for mat_R.